

THESIS FOR THE DEGREE OF LICENTIATE OF ENGINEERING

**Molecules at stellar death: from the winds of  
massive evolved stars to supernova remnants**

SOFIA WALLSTRÖM



**CHALMERS**

Department of Earth and Space Sciences  
CHALMERS UNIVERSITY OF TECHNOLOGY  
Göteborg, Sweden 2013

## **Molecules at stellar death: from the winds of massive evolved stars to supernova remnants**

SOFIA WALLSTRÖM

© Sofia Wallström, 2013

Radio Astronomy & Astrophysics Group  
Department of Earth and Space Sciences  
Chalmers University of Technology  
SE-412 96 Göteborg, Sweden  
Phone: +46 (0)31-772 1000

### **Contact information:**

Sofia Wallström  
Onsala Space Observatory  
Chalmers University of Technology  
SE-439 92 Onsala, Sweden

Phone: +46 (0)31-772 5544  
Fax: +46 (0)31-772 5590  
Email: [sofia.wallstrom@chalmers.se](mailto:sofia.wallstrom@chalmers.se)

### **Cover image:**

*Spectra over the Herschel PACS footprint, showing CO J=23-22 in blue and [O III] 88 $\mu$ m in red, overlaid on a Spitzer/IRAC image of the CO vibrational emission in Cas A.  
Image credits: Wallström et al. (2013)*

Printed by Chalmers Reproservice  
Chalmers University of Technology  
Göteborg, Sweden 2013

# Molecules at stellar death: from the winds of massive evolved stars to supernova remnants

SOFIA WALLSTRÖM

Department of Earth and Space Sciences

Chalmers University of Technology

## Abstract

Massive stars play a key role in the chemical and dust budget of the galaxy, producing heavy elements, molecules, and dust. At the end of their lives they evolve through stages of significant mass-loss, which affect the subsequent evolution of the star, including whether or not it will eventually explode as a supernova (SN). To contribute to the understanding of this cycle, we aim to use molecular emission as a probe of the physical conditions and kinematics of the gas in the envelopes of evolved massive stars and supernova ejecta. This will allow us to better understand the mechanisms at work in these complex environments. For this purpose, we have studied two peculiar objects. First is the evolved star IRAS 17163, a recently identified member of the rare Yellow Hypergiant (YHG) class, and one of the few with a massive dusty envelope. To probe its mass-loss and circumstellar kinematics, low-J CO lines were observed with APEX. The observations show a complex line profile, with multiple peaks and a broad underlying component, which is significantly redshifted from observed optical line velocities. This phenomenon is as yet unexplained, and further work aims to disentangle the various velocity components and determine the circumstellar structure.

Second is a knot in the supernova remnant (SNR) Cas A, the first SNR to exhibit CO emission, in which several high-J CO lines were observed with *Herschel*. A large column density of warm and dense CO was found, which, along with the broad linewidths, implies that the emission originates in the post-shock region of the reverse shock. As molecules are thought to be destroyed by the reverse shock, the observed CO emission supports the predictions of chemical models that find a significant mass of CO can reform after the passage of the reverse shock. Studying the gas characteristics around the reverse shock also constrains dust survival in SNRs, with implications for explaining the large dust masses seen in the early universe.

In both cases, the molecular emission provides vital information of the gas conditions and kinematics, allowing us to understand the evolution of these objects and the impact they have on their surroundings. Further study will require higher angular resolution, in order to resolve the complex gas structures, and hence the use of interferometers such as the exceptional new ALMA telescope.

**Keywords:** circumstellar matter – stars: AGB and post-AGB – stars: mass-loss – stars: individual: IRAS 17163–3907 – ISM: supernova remnants – submillimeter: ISM – ISM: individual objects: Cassiopeia A



## Research contributions

This thesis is based on the work contained in **Papers I & II**:

- I. S.H.J. Wallström, S. Muller, E. Lagadec, J.H. Black, K. Justtanont, R. Oudmaijer, H. van Winckel & A. Zijlstra:  
*Investigating the nature of the Fried Egg nebula: Further evidence for a yellow hypergiant classification*  
Astronomy & Astrophysics, submitted (2013)
- II. S.H.J. Wallström, C. Biscaro, F. Salgado, J.H. Black, I. Cherchneff, S. Muller, O. Berné, J. Rho & A.G.G.M.Tielens :  
*CO rotational line emission from a dense knot in Cassiopeia A: Evidence for active post-reverse-shock chemistry*  
Astronomy & Astrophysics, 558, 2 (2013)



## Acknowledgements

First, a big thank you to my supervisor Sebastien Muller for his patience, help, and encouragement. Thank you also to my second supervisor John Black for his infinite wisdom. Thank you to everyone at the observatory, especially my fellow PhD students, for making it an absolutely lovely place to work. I can't wait for the next 2.5 years!

I would also like to thank the ESF EuroGENESIS research programme for financing my PhD, and the other members of the CoDustMas project for the interesting discussions and new perspectives. Thank you to all my collaborators, for sharing their knowledge and broadening mine.

Finally, thank you to my family, and Shane, for their unwavering support.

Sofia



# Contents

Abstract . . . . .	i
Research contributions . . . . .	iii
Acknowledgements . . . . .	v
<b>1 Introduction</b>	<b>1</b>
1.1 Stars and molecules . . . . .	1
1.1.1 Stellar properties . . . . .	2
1.2 Molecules as observational tools . . . . .	3
1.2.1 Telescopes . . . . .	3
1.2.2 Molecular emission . . . . .	6
1.2.3 Rotation diagram . . . . .	8
1.2.4 RADEX . . . . .	9
<b>2 Molecules in the winds of massive evolved stars</b>	<b>11</b>
2.1 Yellow Hypergiants . . . . .	11
2.1.1 IRAS 17163–3907 . . . . .	14
2.2 Introduction to Paper I . . . . .	14
2.2.1 Future prospects . . . . .	15
<b>3 Molecules in supernova remnants</b>	<b>17</b>
3.1 Supernovae . . . . .	17
3.1.1 SN 1987A . . . . .	18
3.1.2 Molecules and dust in supernova ejecta . . . . .	18
3.1.3 Cassiopeia A . . . . .	19
3.2 Introduction to Paper II . . . . .	20
3.2.1 Heating mechanisms . . . . .	21
3.2.2 Future prospects . . . . .	22
<b>References</b>	<b>25</b>
<b>Paper I</b>	<b>27</b>

**Paper II**

**29**

# Chapter 1

## Introduction

### 1.1 Stars and molecules

When we think of the universe we tend to think of stars, from the constellations in the night sky to glittering images of star-filled galaxies. It's not a complete picture of the universe, but it is a good starting point given that stars are essentially the little engines of our galaxy. Stars provide energy and ionizing radiation to the surrounding gas of the interstellar medium (ISM), and, more importantly, stars have created every atom heavier than hydrogen and helium (called metals, in astronomy) that exists in the universe.

Stars gain their energy from nucleosynthesis in their cores, fusing lighter atoms into heavier atoms, up to iron. These metals are then expelled into the ISM via stellar winds. At the end of a star's life, if it is heavy enough, it will explode as a supernova. Here, in the ejected stellar material, explosive nucleosynthesis can create all the atoms heavier than iron. The ejected material, replete with metals, will expand and eventually integrate into the ISM.

From metals, a wide variety of molecules and dust grains can form, which affect the gas chemistry and provide important cooling mechanisms for the gas. Molecular transitions are a main cooling mechanism at low temperatures, allowing dense molecular clouds to cool, fragment, and collapse to form stars. Without molecules this process would be much less efficient, and incapable of forming low-mass stars. Hence molecules provide an important link in the stellar lifecycle.

Molecules are also useful observationally, as tracers of gas. By observing molecular transitions we can probe a wide variety of gas phases, from stellar winds to supernova remnants. Molecular observations let us study gas kinematics, excitation, and chemistry. It is an important tool for studying various stages of stellar life, from birth to death.

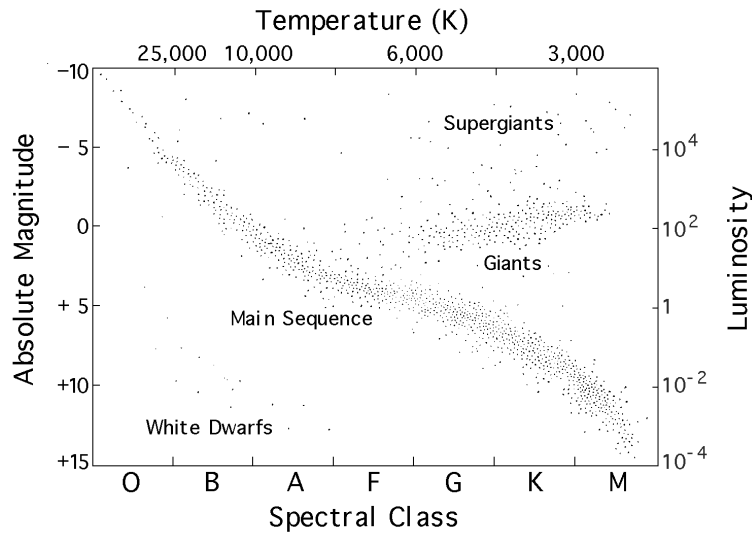


Figure 1.1: The Hertzsprung-Russell diagram of nearby stars. Luminosity is given in solar luminosities,  $L_{\odot}$ . *Image credit: NASA/HEASARC*

### 1.1.1 Stellar properties

Stars are born from the collapse of dense molecular clouds, gathering gas until they are heavy and hot enough to ignite nuclear fusion. Stars can be born with a wide range of masses, which can be approximated by the Salpeter initial mass function (IMF):  $N(m) \propto m^{-2.35}$ , where  $N(m)$  is the number of stars of mass  $m$ . This means that low-mass stars are significantly more numerous than high-mass stars. Mass is an important property for studying a star, along with its surface temperature and luminosity.

In order to classify stars, one can look at their locations in the Hertzsprung-Russell (HR) diagram (Figure 1.1). This is a plot of luminosity against temperature, and a star's location on the HR diagram indicates both its mass and evolutionary status. Most stars are on a "main sequence", which corresponds to the main, hydrogen-burning part of a star's life. Stars with high temperatures and luminosities (high-mass stars) are on the blue (left) end of the main sequence, while stars with low temperatures and luminosities (low-mass stars) are on the red (right) end. After a star has depleted the hydrogen in its core it contracts, heating up, until the core is hot enough to start burning helium. The hot core causes the surrounding layers to inflate, so the star moves off the main sequence and up in the HR diagram towards larger luminosities. This will happen sooner the more massive the star is. There are many tracks a star may follow in the HR diagram, depending on its physical parameters, but generally low-mass stars will come around to the white dwarf branch while high-mass

stars instead end their lives as supernovae.

## 1.2 Molecules as observational tools

Molecules are an important tool for probing cold/cool gas ( $T < 100$  K). They are fairly easily excited and emit radiation at radio frequencies, which can penetrate the atmosphere and are hence observable from the Earth (see § 1.2.1 and Figure 1.3). Radio frequencies also allow for good velocity resolution, through the use of heterodyne spectrometers with resolving power,  $R = \nu / \Delta\nu$ , of up to  $10^7$ , corresponding to a velocity resolution ( $\Delta v = c \Delta\nu / \nu$ ) of  $0.03 \text{ km s}^{-1}$ . Hence, molecular lines allow us to study gas kinematics in high detail, and the line excitation probes the physical conditions of the gas. Observing several different molecules can also elucidate the gas chemistry, helping to constrain astrochemical models.

Molecular gas makes up about 20% of the mass of the ISM (Tielens 2005), and the most common molecule by far is  $\text{H}_2$ , since most atoms in the universe are hydrogen. As  $\text{H}_2$  is a symmetric molecule it has zero dipole moment and hence no allowed rotational transitions, so it is not easily detected in cold gas (see § 1.2.2). Instead we rely on tracer molecules to study the ISM. Over 150 molecules have been detected in space so far, but one of the most observationally useful is carbon monoxide (CO).

CO is the second most common molecule in the universe, with an abundance of  $\sim 10^{-4}$  (relative to  $\text{H}_2$ ) in the ISM. It forms readily, and is very stable due to the triple bond between the carbon and oxygen atoms. CO is a heterogeneous diatomic molecule, with a dipole moment of 0.122 D, so it has a range of low-frequency rotational transitions (Figure 1.2). The dipole moment of CO is small in absolute terms, and hence the emission lines are not as intrinsically strong as the lines of other molecules, but the large CO abundance (orders of magnitude greater than other ISM molecules) overcomes this and CO lines are readily observable. The lowest transitions are easily excited in cold ISM gas ( $E_{up} < 30$  K, see Figure 1.2), allowing us to study e.g. Giant Molecular Clouds, while the higher transitions trace warmer, denser gas, such as might be found in shocks around stars. CO also has several common isotopologues (e.g.,  $^{13}\text{CO}$ ,  $\text{C}^{18}\text{O}$ ,  $\text{C}^{17}\text{O}$ ) that can be used to probe large column densities of gas, which are optically thick in the main  $^{12}\text{C}^{16}\text{O}$ .

### 1.2.1 Telescopes

In order to observe the emission or absorption from interstellar molecules, we need large and powerful telescopes. The diameter of a single dish telescope,  $D$ , determines its sensitivity (collecting area) and angular resolution ( $\sim \lambda / D$ ), so as large a telescope as possible is the ideal. However, the required surface

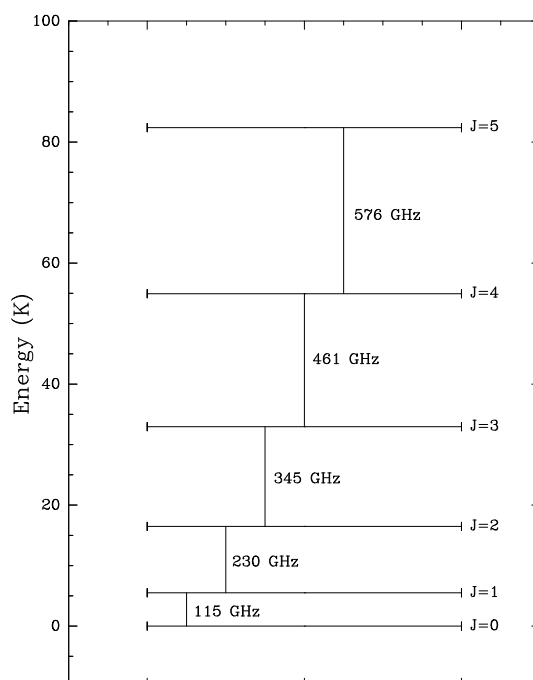


Figure 1.2: First few pure rotational energy levels of CO, and the transition frequencies.

accuracy of the dish is smaller than the wavelength of the radiation, so as we aim for higher energy transitions at higher frequencies (shorter wavelengths), the maximum dish size is limited.

One way around this problem is to use the technique of radio interferometry. Interferometry correlates the data from multiple antennae to “synthesize” a single dish as large as the maximum distance between the antennae (called the baseline). This is a powerful technique, allowing us to reach resolutions of less than a milliarcsecond, though the complicated image synthesis means that data interpretation can be difficult.

Another observational challenge is the Earth’s atmosphere. The atmosphere absorbs most of the radiation that hits it, though there are transmission “windows” in the optical/near-IR and radio parts of the spectrum (Figure 1.3), which allow radiation through. Furthermore, fluctuations in the atmosphere distort observations, even in the atmospheric windows. So to get around the problems of the atmosphere, telescopes can either be put on mountains, above as much of the atmosphere as possible, or in space.

For observing pure rotational CO emission, the required wavelengths range between  $\sim 1$  mm and  $100 \mu\text{m}$ . At these wavelengths the atmosphere’s opacity is strongly affected by water vapor, and the effect increases with shorter wavelengths. Around  $100 \mu\text{m}$  the atmosphere is completely opaque. Hence, low-J

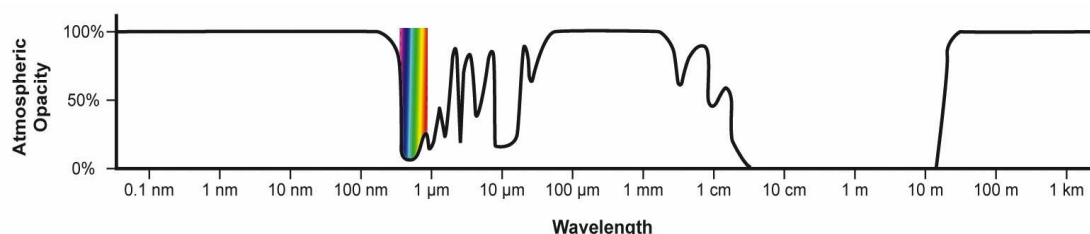


Figure 1.3: The opacity of the atmosphere at different wavelengths. Most radiation is absorbed completely (opacity 100%) except for windows at optical/near-IR ( $\sim 1 \mu\text{m}$ ) and radio (1 cm–10 m) wavelengths. *Image credit: NASA/IPAC*

CO transitions ( $J < 10$ ) require a telescope site that is both high and dry, while high- $J$  transitions require a space telescope. Some examples of mm/submm telescopes relevant to this thesis are presented below.

### APEX

The Atacama Pathfinder EXperiment (APEX)<sup>1</sup> is a 12m mm/submm telescope located at Llano de Chajnantor in the Atacama desert in northern Chile, at an elevation of 5100 m. It is operated jointly by the Onsala Space Observatory (OSO), Max Planck Institut für Radioastronomie (MPIfR) and the European Southern Observatory (ESO). The high altitude and dry and stable atmosphere makes the location ideal for a mm/submm telescope. The CO data for Paper I were obtained with APEX, with the heterodyne receivers at 230 and 345 GHz (corresponding to wavelengths around 1 mm). The spectral resolution of the receivers is  $\sim 0.1 \text{ km s}^{-1}$  at these frequencies, though we have smoothed our data to a resolution of  $1 \text{ km s}^{-1}$ .

### Herschel

The *Herschel* Space Observatory<sup>2</sup> was launched into orbit in May 2009, as part of the European Space Agency (ESA) science programme. It is a 3.5m telescope, the largest ever flown in space, with imaging and spectroscopic instruments operating in the 55–671  $\mu\text{m}$  infrared wavelength range. The data for Paper II were obtained with *Herschel*, using the Photodetector Array Camera and Spectrometer (PACS) instrument. PACS has a field of view of  $\sim 50' \times 50'$ , divided into a 5x5 array of pixels. We observed several CO transitions in the wavelength range 87–186  $\mu\text{m}$ , with a spectral resolution around  $\sim 175 \text{ km s}^{-1}$ .

<sup>1</sup><http://www.apex-telescope.org/>

<sup>2</sup><http://www.esa.int/herschel>

## ALMA

The Atacama Large Millimeter/submillimeter Array (ALMA)<sup>3</sup> is an interferometer in the final stage of construction (Early Science), located at Llano de Chajnantor next to APEX. It is an international collaboration between Europe, North America, East Asia, and Chile. When completed, ALMA will have baselines of up to 16km, allowing for high angular resolution (0.006"), and 50 12m dishes to provide excellent sensitivity as well. There are observing bands between 84 and 720 GHz, which cover several rotational CO transitions and myriad transitions in other molecules.

### 1.2.2 Molecular emission

*General reference: Wilson (2009)*

As a consequence of quantum mechanics, the energy levels of molecules are discrete. Transitions between these levels result in the emission of electromagnetic radiation at specific frequencies, the observation of which lets us deduce something about the physical conditions of the molecule. There are three types of molecular emission: electronic, vibrational, and rotational.

Electronic emission involves the transitions of electrons between energy levels. These transitions have typical energies of a few electron volts (eV), which corresponds to radiation in the visible and UV parts of the electromagnetic spectrum, with wavelengths around 100 nm. Vibrational emission involves the bonds between the atoms stretching and bending, and is mainly in the infrared (IR) part of the spectrum, with wavelengths of several  $\mu\text{m}$ . Rotational emission is due to transitions between the quantized rotational states of the molecule and is seen in the radio/sub-mm part of the spectrum, with typical wavelengths around 1 mm.

For illustration, the simple case of rotation in a linear diatomic molecule (with zero net electron spin) can be mathematically described as follows: a linear molecule can be approximated as a rigid rotor, so the energy of rotational state  $J$  above the ground state is given by

$$E = hB_0J(J + 1) \quad (1.1)$$

where  $J$  is the angular momentum quantum number, and  $B_0$  is the rotational constant. Only rotational transitions with  $\Delta J=1$  are allowed by the quantum mechanical selection rules. The corresponding transition frequencies are about  $\nu = \Delta E/h = 2B_0(J + 1)$ . The state energy is associated with a temperature, given by  $E/k_B$ , in Kelvin.

---

<sup>3</sup><http://www.almaobservatory.org/>

The probability for a molecule to spontaneously transition from the  $J+1$  to  $J$  state ( $u$  to  $l$ ) is given by the Einstein A coefficient

$$A_{ul} = \frac{64\pi^4}{3hc^3} \nu^3 |\mu_{ul}|^2 \quad (1.2)$$

where  $A_{ul}$  is in  $\text{s}^{-1}$ , and  $\mu_{ul}$  is the dipole moment, which is the product of charge and the separation of charges so it is analogous to classical angular momentum. The dipole moment  $|\mu_{ul}|^2$  can be expressed by its radial part  $\mu$  as:

$$|\mu_{J+1 \rightarrow J}|^2 = \mu^2 \frac{J+1}{2J+3} \quad (1.3)$$

giving

$$A_{ul} \simeq 1.165 \times 10^{-11} \mu^2 \nu^3 \frac{J+1}{2J+3} \quad (1.4)$$

where  $\nu$  is the transition frequency in GHz, and  $\mu$  is in Debye.

The Einstein A coefficient gives the probability for the upper level to decay to the lower level by spontaneous emission of a photon. Hence, the inverse gives an estimate of the lifetime of the upper state. Typical values of  $A_{ul}$  for interstellar molecules are  $10^{-8}$ – $10^{-3} \text{ s}^{-1}$ , corresponding to upper level lifetimes ranging from hours to years.

In order for a molecule to emit radiation by decaying to a lower level, it must first be excited to an upper level. Molecules can be excited by absorbing radiation or from collisions with surrounding particles (most likely  $\text{H}_2$ ). The main excitation mechanism for a given molecule depends on the structure of the molecule itself, e.g., the energy level spacing, as well as its surroundings: the density of the surrounding gas and the strength of the background radiation field.

In a two level system, consisting of an upper level  $u$  and a lower level  $l$ , the populations of the levels are set by the rates of collision, absorption, and spontaneous and stimulated emission. At statistical equilibrium ( $dn_i/dt=0$ ), in the absence of chemical sources or sinks:

$$\frac{n_u}{n_l} = \frac{nq_{lu} + B_{lu}I}{nq_{ul} + A_{ul} + B_{ul}I} \quad (1.5)$$

$$A_{ul} = \frac{8\pi h\nu^3}{c^3} B_{ul}$$

with  $n$  the gas density, and  $I$  the radiation density.  $q_{ij}$  are the collisional coefficients, and  $B_{ij}$  the stimulated emission/absorption coefficients.

For a more intuitive understanding, we can define two temperatures,  $T_{ex}$  and  $T_k$ , by

$$\frac{q_{lu}}{q_{ul}} = \frac{g_u}{g_l} \exp\left(-\frac{T_0}{T_k}\right), \text{ with } T_0 \equiv \frac{h\nu}{k_B} \quad (1.6)$$

$$\frac{n_u}{n_l} = \frac{g_u}{g_l} \exp\left(-\frac{T_0}{T_{ex}}\right) \quad (1.7)$$

The kinetic temperature  $T_k$  is the physical temperature of the gas. The excitation temperature  $T_{ex}$  is the temperature at which we would expect to find this ratio of level populations, according to a Boltzmann distribution. Note that  $T_{ex}$  is not necessarily a physical temperature: it can take a wide range of values and can even be negative when level populations are inverted, as in masers.

In radio astronomy, we also define another temperature for the intensity of the emission. For a brightness  $I$  in units of  $\text{W m}^{-2} \text{Hz}^{-1} \text{sr}^{-1}$ , the brightness temperature,  $T_b$  is defined as

$$T_b = \frac{\lambda^2}{2k_B} I \quad (1.8)$$

which is the temperature of a black body of brightness  $I$ , in the Rayleigh-Jeans approximation (when  $h\nu \ll k_B T$ ) which applies well to emission with wavelengths on the order of meters to centimeters.

In general,  $T_k$ ,  $T_{ex}$ , and  $T_b$  can be different. Substituting these quantities into equation 1.5 we find an expression for  $T_{ex}$ :

$$T_{ex} = T_k \frac{T_b A_{ul} + T_0 n q_{ul}}{T_k A_{ul} + T_0 n q_{ul}} \quad (1.9)$$

If collisions dominate the excitation, i.e., if  $n q_{ul} \gg A_{ul}$ ,  $T_{ex}$  tends towards  $T_k$ . Under these conditions the gas is in local thermal equilibrium (LTE), and can be defined by a single equilibrium temperature, equal to  $T_{ex} = T_k$ . If radiation dominates the excitation, and  $n q_{ul} \ll A_{ul}$ ,  $T_{ex}$  will instead tend towards  $T_b$ . The density at which collisions and radiation have roughly equal contributions is called the critical density,  $n_c \simeq A_{ul}/q_{ul}$ . As  $A_{ul}$  depends on the transition frequency, different transitions of the same molecule will have different  $n_c$ , increasing with  $J$ . In general, if an environment satisfies  $n > n_c$  and  $T > E_u/k_B$  for a given molecular transition, we expect that transition to be excited. Whether we can detect this emission, however, depends on further factors, including the abundance of the molecule.

### 1.2.3 Rotation diagram

As discussed above, at densities greater than the critical density,  $n_c$ , we can assume the emitting gas is in LTE and can hence be described by a single temperature:  $T_{ex} = T_k$ . If we have observations of more than one transition of the same molecule, we can derive this temperature and the total column density (molecules per unit area) of the molecule. This is done by creating a rotation diagram, as described by Goldsmith & Langer (1999) and summarized below.

It can be shown that the integrated intensity,  $I_{ul}$ , of an optically thin emission line is related to the population density of the upper energy level,  $N_u$ , by

$$\int I_{ul} = \frac{N_u A_{ul} h \nu_{ul}}{4\pi} \quad (1.10)$$

where  $A_{ul}$  is the Einstein coefficient for the  $u \rightarrow l$  transition. Hence we can derive  $N_u$  from line observations.

In LTE, the energy level populations follow a Boltzmann distribution, so that

$$N_u = \frac{N}{Z} g_u e^{-E_u/T_{ex}} \quad (1.11)$$

where  $N$  is the total column density,  $Z$  is the partition function,  $g_u$  is the statistical weight of the upper level  $u$ , and  $E_u$  is the energy of the upper level in Kelvins.

If we take the logarithm of this equation we get a simple linear relation between  $\ln N_u/g_u$  and  $E_u$ :

$$\ln \frac{N_u}{g_u} = \ln \frac{N}{Z} - E_u/T_{ex} \quad (1.12)$$

Plotting this relation for all observed transitions of a molecule will allow us to derive the excitation temperature,  $T_{ex}$ , from the slope of the line, and the total column density of the molecule,  $N$ , from the y-intercept. This method is fast and straightforward (if the emission lines are optically thin), but it does rely on the assumption that the gas an ideal two-level system in LTE.

#### 1.2.4 RADEX

There are ways of determining the temperature and density of a molecule without the assumption of LTE, and one of the most straightforward is implemented in the freely available RADEX<sup>4</sup> program (van der Tak et al., 2007). RADEX calculates the non-equilibrium excitation levels of a molecule by assuming a uniform emitting region (i.e., constant density, temperature, and abundance). It requires the collisional rates between the molecule and a collision partner (usually H<sub>2</sub>, but can also be, e.g., H<sub>2</sub>O or electrons), which are available for about a dozen different molecules in the LAMDA<sup>5</sup> molecular database.

RADEX takes as input parameters the density of the collision partner, and the column density and kinetic temperature of the molecule. It then iteratively solves for the level populations and the radiation field, stopping when the calculated optical depths are stable from one iteration to the next. By testing a range of input parameters, one can fit the line strengths predicted by RADEX to

<sup>4</sup><http://www.sron.rug.nl/~vdtak/radex/radex.php>

<sup>5</sup><http://home.strw.leidenuniv.nl/~moldata/molecules.html>

observed data, thereby constraining the density, column density, and kinetic temperature of the gas without an assumption of LTE. This is extremely useful as an approximation of the physical parameters of an observed molecule.

# Molecules in the winds of massive evolved stars

When massive stars near the end of their lives, their stellar winds become very vigorous, ejecting up to  $10^{-3} M_{\odot}$  of material per year. Such stars have a huge impact on their surroundings, despite their rarity. Molecules can be used as tracers of this wind, probing the mass-loss rate and the kinematics of the gas. A commonly observed molecule is CO, due to its abundance and excellent observational properties, as discussed in § 1.2. The distribution of this circumstellar gas will affect the future evolution and (very likely) explosion of a massive star as a supernova, so studying these late evolution stages is vital to understanding the life and death of massive stars.

## 2.1 Yellow Hypergiants

*General references: Oudmaijer et al. (2009); de Jager (1998)*

When stars of mass  $>8 M_{\odot}$  run out of hydrogen in their cores at an age of  $\sim 10^7$  years, they move off the main sequence to become Red Supergiant (RSG) stars. This stage, and later evolutionary stages, are characterized by intense mass-loss. This mass-loss shapes the circumstellar envelope, later forming planetary nebulae, for example, or controlling the geometry of an eventual supernova explosion. The amount of mass lost actually determines whether the star explodes as a supernova at all, because if it loses too much mass the core will not be heavy enough to collapse catastrophically.

After the RSG branch, a massive star can evolve in several ways depending on its composition and other characteristics. Some stars make "excursions" around the HR diagram, eventually returning to the RSG branch. Others evolve

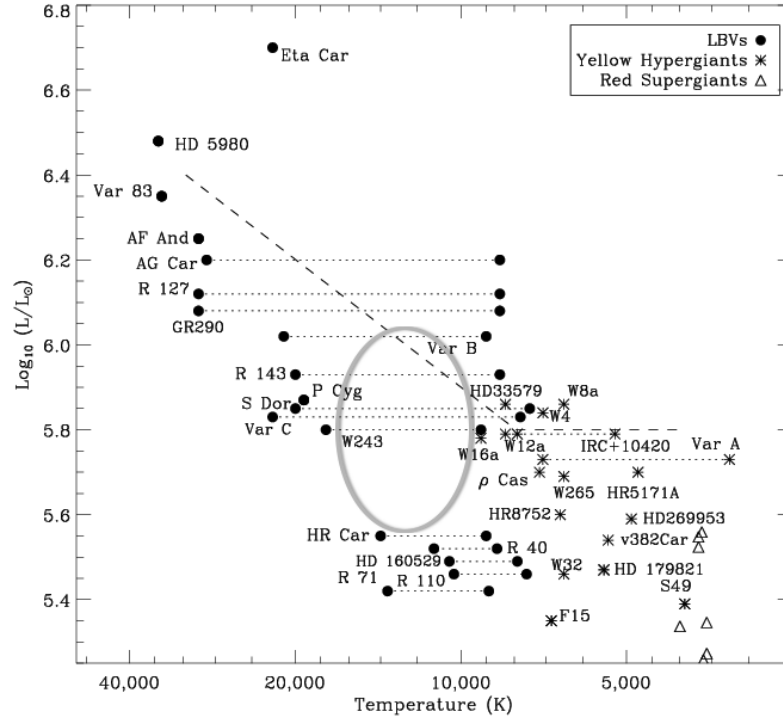


Figure 2.1: The high-luminosity part of the HR diagram, where the Yellow Hypergiants are found. The approximate location of the Yellow Void is indicated with a grey ellipse. *Image credit: Oudmaijer et al. (2009).*

into Luminous Blue Variable (LBV) and then Wolf Rayet (WR) stars, which are very hot stars losing a lot of mass via fast stellar winds. In the middle of the RSG to WR evolution, which is expected to take several hundred to a few thousand years (Garcia-Segura et al., 1996), there is the Yellow Hypergiant (YHG) stage. The number of known Yellow Hypergiant stars is small, partly because of the short duration of the YHG stage, and partly because they are difficult to identify. Part of the definition of a YHG star is an absolute magnitude,  $M_V$ , brighter than  $-7$ , and the determination of  $M_V$  requires an accurate distance measurement. Another defining feature of YHGs is broad  $H\alpha$  emission components, which implies large-scale photospheric motion and an extended envelope. This, in turn, implies a large mass-loss rate. So YHGs are intrinsically bright, with typical luminosities around  $10^6 L_\odot$ , and losing a lot of mass. They have temperatures between  $\sim 7000\text{--}10\,000$  K, so on the HR diagram they lie between RSGs and LBV/WR stars (Figure 2.1).

There is a gap in the HR diagram, an area with very few stars just bluewards of the YHGs, called the Yellow Void. The Yellow Void is believed to be

associated with inherently unstable stellar parameters, so that YHGs evolving towards it will not be able to enter the Void, and will instead “bounce” back redwards. This “bouncing” against the Yellow Void is another unique characteristic of the Yellow Hypergiants. “Bounces” have been observed to be associated with periods of increased mass-loss, which are believed to cause the subsequent redward motion: the wind becomes optically thick, essentially forming a cool pseudo-photosphere around the star. After the wind clears, the star can once again move towards the Yellow Void, until its photosphere becomes unstable and it enters another period of increased mass-loss. The star HR 8752, for example, has undergone at least two “bounces” over a period of 30 years (de Jager & Nieuwenhuijzen, 1997).

The photospheric instability of the Yellow Void is associated with the effective photospheric acceleration,  $g_{eff}$ . When  $g_{eff}$  is close to zero, as is the case at the Yellow Void, the atmosphere is more or less detached from the star’s gravitational attraction. This means the star will pulsate with supersonic velocity amplitudes, allowing for ejection of gas at supersonic speeds and greatly enhanced mass-loss during part of the pulsation cycle. The pulsation period is typically  $\sim 500$  days, so the star can eject huge amounts of gas on a timescale of about a decade.

It is thought that once a YHG has ejected enough mass its stellar envelope will be able to survive the instabilities of the Yellow Void, and the star will evolve to become an LBV on the other side of the Void. Hence the YHG stage links the comparatively well understood RSG and LBV/WR phases, both evolutionarily and with regard to the formation of circumstellar structures. It is important to study YHGs for this reason, despite the short duration of the phase, but the varied properties of YHG stars poses a challenge.

The variation in the properties of YHGs is caused by the movement of the stars in the HR diagram, and their “bouncing” against the Yellow Void, but they have a few features in common: large luminosities, and large mass-loss rates. This, combined with their past RSG phase, means all YHGs should have significant circumstellar envelopes. But very few have been found to have extended shells. The famous  $\rho$  Cas, for example, shows no extended emission.

The archetypal YHG, IRC+10420, is one of the few that shows extended circumstellar shells. It is also significant in its large outflow velocity ( $\sim 40 \text{ km s}^{-1}$ ) and huge mass-loss rate ( $> 10^{-4} M_{\odot} \text{ yr}^{-1}$ ). On the largest scales, IRC+10420 has largely spherically symmetric circumstellar shells, but closer to the star the more recently ejected features show lots of structure (Castro-Carrizo et al., 2007). They appear to have been ejected by short bursts of mass-loss in random directions, perhaps indicative of explosive “bounces” against the Void. Another of the few YHGs with extended circumstellar shells is the newly reclassified IRAS 17163–3907 (IRAS 17163), which is the subject of Paper I.

### 2.1.1 IRAS 17163–3907

IRAS 17163 was only recently identified as a Yellow Hypergiant star, despite being one of the brightest infrared sources in the sky, because its distance was not well constrained. The star was discovered by Henize (1976), and classified as a post-AGB star by Le Bertre et al. (1989). They assumed a distance less than 1 kpc based on a positive radial velocity, inconsistent with galactic rotation, which means the star is most likely in the solar neighborhood. The close distance was backed up by the fact that the star was resolved by IR speckle interferometry.

However, a new distance measurement was made by Lagadec et al. (2011) based on interstellar absorption lines in the optical spectrum of IRAS 17163. The absorption line velocity suggests the absorbing gas is 3.6 kpc away, if it follows Galactic rotation, giving a lower limit on the distance to the star. An upper limit on the distance was also derived, based on the maximum visual extinction, to be 4.7 kpc. The new distance of  $\sim 4$  kpc also increases the derived luminosity of the star to  $5 \times 10^5 L_{\odot}$ , placing IRAS 17163 among the Yellow Hypergiants on the HR diagram.

The YHG status of IRAS 17163 is further backed up by dust measurements: Lagadec et al. (2011) found two concentric spherical dust shells within  $5''$  of the star using mid-IR observations, with a huge warm ( $\sim 200$  K) dust mass of  $0.04 M_{\odot}$ , inspiring the nickname the Fried Egg nebula. Hutsemékers et al. (2013) used *Herschel* to look in the far-IR and discovered a  $50''$  dust ring around the star containing  $\sim 0.17 M_{\odot}$  of cool ( $\sim 60$  K) dust. This implies a total ejected mass of at least  $10 M_{\odot}$ , depending on the assumed gas-to-dust mass ratio (here: 50), over the past  $\sim 10\,000$  years. The  $50''$  ring was most likely ejected during the RSG phase, but the warm dust close to the star is estimated to have been ejected in several mass-loss episodes within the past  $\sim 400$  years, consistent with the YHG phase. Further evidence IRAS 17163 is a Yellow Hypergiant, along with CO observations of its circumstellar material, is presented in Paper I.

## 2.2 Introduction to Paper I

In order to probe the kinematics of the circumstellar envelope and constrain the mass-loss rate, IRAS 17163 was observed in CO (2–1) and (3–2) using the APEX telescope. A complex CO line shape was found around  $+65 \text{ km s}^{-1}$ , consisting of two peaks and a broad underlying component.

An optical spectrum from the Mercator telescope is also presented, and compared with the optical spectrum of the archetypal YHG IRC+10420. The similarity between the two spectra further supports the classification of IRAS 17163 as a Yellow Hypergiant. The optical lines have velocities around  $+18 \text{ km s}^{-1}$ , significantly offset from the CO emission. This phenomenon is as yet unexplained.

### 2.2.1 Future prospects

In trying to understand the complex CO emission, further APEX observations were obtained. These were in a line across IRAS 17163, with pointings at  $(\pm 25'', 0)$ ,  $(\pm 20'', 0)$  and on the star. The observations show a velocity gradient of  $\sim 10 \text{ km s}^{-1}$  across the star, from West to East, centered around  $+65 \text{ km s}^{-1}$ . More surprisingly, the sum of the  $(\pm 20'', 0)$  spectra matches the spectrum taken on the star, implying that the emission is concentrated in the overlap regions between these pointings. This, along with the velocity gradient, suggests there is some sort of bipolar outflow from the star. However, this is at odds with the very symmetric dust rings at both  $5''$  and  $50''$  from the star. Furthermore, there is still an unexplained discrepancy between the optical and CO line velocities.

The limited number of pointings around IRAS 17163 only allows for a limited understanding of the complicated circumstellar structure. Mapping the entire envelope will allow for a more complete understanding of the kinematics and excitation of the circumstellar gas, and help disentangle the various gas components: the warm, recently ejected gas within  $5''$ ; the cool  $50''$  ring; and the potential bipolar outflow. To this end, we have submitted a proposal to APEX to map the star and its surroundings in CO 2–1 and 3–2.

Further study will require even greater angular resolution, to resolve the circumstellar gas structure. To that end, we will also submit a proposal to ALMA to map the stellar envelope.



# Molecules in supernova remnants

## 3.1 Supernovae

When stars of initial mass greater than  $\sim 8 M_{\odot}$  reach the end of their  $\sim 10$ -million-year lives they explode as core-collapse<sup>1</sup> supernovae (SNe). The core collapses into a neutron star or black hole, while the outer layers of the star are ejected at enormous speeds ( $\sim 20\,000 \text{ km s}^{-1}$ ). The explosion releases a huge amount of energy:  $10^{51}$  ergs, or about as much as the Sun will produce throughout its  $\sim 10$  billion year lifetime. Some of the ejected material (ejecta) undergoes explosive nucleosynthesis, which is the source of most of the elements heavier than iron found in the Universe, including on Earth. Elements with masses up to and including that of iron are also present in the ejecta, having formed in the star during its lifetime. The ejecta expand outwards, pushing before it a shock wave which interacts with the circumstellar material expelled by the progenitor star, and then the ISM surrounding it. The shock wave will heat the gas it encounters to millions of degrees, ionizing it, and will destroy dust by sputtering (bombarding solid material with fast particles causes atoms to be ejected from the solid). When this forward shock wave has swept up a mass similar to the ejecta mass, a reverse shock wave is formed, and the object is now called a supernova remnant (SNR). This reverse shock travels back inwards towards the explosion centre at  $\sim 2000 \text{ km s}^{-1}$ , interacting with the ejecta as it goes. When the reverse shock hits the ejecta, the material will be slowed, heated, dissociated, and ionized. The fate of the supernova ejecta is very interesting as it contains large amounts of heavy elements, and understanding the effect of the reverse shock is crucial to determining this fate.

---

<sup>1</sup>Henceforth I will use the term supernova to mean specifically core-collapse supernova, which is caused by the collapse of a massive star, as I will not discuss the other type of supernova (type Ia, caused by a white dwarf star exceeding its Chandrasekhar mass).

### 3.1.1 SN 1987A

February 23<sup>rd</sup>, 1987, was a very special day for the astronomical community. On this day, the light (and also neutrinos!) from a supernova in the Large Magellanic Cloud, a satellite galaxy to the Milky Way, reached us. It is the nearest supernova that has occurred since we've had the capability of studying them in detail, so SN 1987A (so named because it was the first observed supernova in 1987) was extensively monitored and is still regularly observed today. Much of what we know about core-collapse supernovae comes from observations of SN 1987A. Molecules, CO and SiO, were observed in the SN ejecta some 200 days after the explosion, in vibrational bands, indicating very hot molecules (Danziger et al., 1987; Aitken et al., 1988). However, the molecular emission faded some 600 days later, either because the molecules were destroyed or because they cooled beyond infrared detection. There was also evidence of dust formation in the ejecta from about 500 days post-explosion, seen in the mid-IR (Moseley et al., 1989), with an estimated dust mass of  $\sim 10^{-4} M_{\odot}$ . Recent observations with the far-IR *Herschel* telescope,  $\sim 25$  years after the explosion, have revealed large masses of cold dust and molecules:  $\sim 0.5 M_{\odot}$  of dust (Matsuura et al., 2011) and  $\sim 0.01 M_{\odot}$  of CO (Kamenetzky et al., 2013).

### 3.1.2 Molecules and dust in supernova ejecta

From SN 1987A it is known that dust and molecules are formed soon after the supernova explosion. This is also corroborated by observations of other supernovae (e.g., Kotak et al., 2005, 2006, 2009), so molecule formation is a common occurrence. This is supported by theoretical studies (e.g., Cherchneff & Dwek, 2009), which show that molecules form quickly and in abundance in SN ejecta. Among these molecules are dust precursors, like SiO, which will bind together into clusters and eventually form dust, a process aided by the cooling of the gas through molecular emission. Hence, molecules are very important for deciding the onset, composition, and mass of SN dust. These dust grains will continue to grow and molecules continue to form as the ejecta cools and expands (Sarangi & Cherchneff, 2013), as evidenced by the large dust and molecule masses found in SN 1987A decades after the explosion.

The net production of dust in supernovae, taking into account both dust creation, and dust destruction by the forward and reverse shocks, is the subject of much debate. The interest in this question stems from the huge dust masses which have been observed in the early universe (e.g., Bertoldi et al., 2003; Beelen et al., 2006), in galaxies less than a billion years old. This dust had very little time to form, requiring fast dust production processes. In our galaxy, the main dust producers are the evolved AGB stars, which have already lived for some billions of years before moving onto the AGB branch. These stars most likely cannot produce enough dust quickly enough to explain the high-*z* observations

(Gall et al., 2011). The stars that explode as supernovae, however, are larger and hence have shorter lives, exploding after only  $\sim 10$  million years. They are therefore the prime contenders for explaining the large dust masses. However, this requires that each supernova produce  $\sim 0.1\text{--}1 M_{\odot}$  of dust, which is predicted by theoretical models (e.g., Todini & Ferrara, 2001), but not entirely supported by observations. Observations of warm dust formed some hundreds of days after a supernova find dust masses of only  $10^{-5}$  to  $10^{-2} M_{\odot}$  (e.g., Lucy et al., 1989; Sugerman et al., 2006; Szalai & Vinkó, 2013). On the other hand, observations of older supernova remnants find cold dust masses of  $\sim 0.1 M_{\odot}$  (Barlow et al., 2010; Matsuura et al., 2011). But we still do not know the net dust yields of these supernovae, as some supernova dust may be destroyed by the reverse shock, and the forward shock may destroy pre-existing ISM dust. Hopefully, monitoring young SNRs being reprocessed by the reverse shock will provide better constraints on the net dust yield of supernovae.

### 3.1.3 Cassiopeia A

In order to study dust and molecules in SNRs, the SNR need to be young and near enough that we can distinguish the SN ejecta from the swept up circumstellar and interstellar material. Cassiopeia A (Cas A) is a prime candidate as it is one of the youngest galactic supernovae,  $\sim 330$  years old and 3.4 kpc away. Additionally, the reverse shock has only just started to reprocess the ejecta, so there is the opportunity to study the ejecta both pre- and post-shock. As a nearby SNR, Cas A has been extensively studied at a range of wavelengths, from X-ray to radio. The kinematics of the ejecta have been carefully deduced, and a fairly large mass,  $\sim 0.1 M_{\odot}$ , of cool dust has been found (Rho et al., 2008; Barlow et al., 2010). Cas A is also used by theoreticians as a standard SNR to model, and the abundances of various molecules in the SN ejecta have been calculated using chemical kinetic modeling (e.g., Sarangi & Cherchneff, 2013). Chemical kinetic modeling takes as input the atomic abundances in stratified SN layers from nucleosynthesis modeling, and follows the outcome of almost every conceivable chemical reaction to determine the abundances of various molecules and clusters as a function of post-explosion time. Such studies have determined that molecules such as CO and SiS should be abundant (up to 10% of the total gas mass) in Cas A, which is an oxygen/silicon-rich SNR.

Cas A is the first supernova remnant where CO emission has been observed, hundreds of years after the SN explosion. Rho et al. (2009) used the Wide field InfraRed Camera (WIRC) at the Hale Telescope on Mount Palomar to observe the CO (2-0) ro-vibrational (rotational transitions between different vibrational states) transition at  $2.294 \mu\text{m}$ . They detected CO in many small ( $< 1''$ ) knots at the reverse shock at the north and east of the remnant (Figure 3.1). Rho et al. (2012) followed up with spectroscopic observations, using the *AKARI* InfraRed



Figure 3.1: Composite near-IR image of Cas A, with ro-vibrational CO emission in red. Areas of excess CO, in the north and east, are marked with boxes. *Image credit: Rho et al. (2009).*

Camera (IRC), of the CO fundamental band at  $4.65 \mu\text{m}$ . Using LTE modeling they derive a CO temperature between 1200 and 2400 K, and estimate a total CO mass of  $6 \times 10^{-7} M_{\odot}$ .

The detection of ro-vibrational CO in Cas A paved the way for observations of rotational CO, and hence the determination of the kinetics, temperature, and density of the ejecta gas, as presented in Paper II.

### 3.2 Introduction to Paper II

In order to probe the physical conditions of the ejecta, several rotational transitions of CO were observed in a region in the north-west of the supernova remnant Cas A, at the brightest CO knot found by Rho et al. (2009). The previous observations found that the CO is warm, so we expect high-J rotational transitions to be brighter than low-J transitions. This makes *Herschel* the ideal telescope to use. In the analysis of these data, we use both the rotational diagram method and RADEX-based modeling, as described in § 1.2.3 and § 1.2.4.

We find a large column density ( $\sim 10^{17} \text{ cm}^{-2}$ ) of warm CO, with two temper-

ature components around 500 and 2000 K. The gas density is constrained to be high,  $\sim 10^6 \text{ cm}^{-3}$ , by the RADEX modeling.

### 3.2.1 Heating mechanisms

The CO emission appears to originate in a small knot of warm and dense gas. This implies that the knot will be able to cool quickly through the emission of CO lines. As a result, additional heating is required to explain the observed warm temperature. Several heating mechanisms are discussed in Paper I, and are explained below in more detail.

#### UV heating

The first heating source considered was the shock front of the reverse shock, where UV photons are emitted from the hot gas ( $T > 10^6 \text{ K}$ ). As the ejecta is oxygen rich, we consider a flux of  $F_o = n_o v_s$  ( $n_o$ =oxygen density;  $v_s$ =shock velocity) oxygen atoms flowing into the shock. From Borkowski & Shull (1990) we adopt the model closest to our assumed shock velocity of  $200 \text{ km s}^{-1}$ , which is their model G with a velocity of  $170 \text{ km s}^{-1}$ . The emergent UV flux they calculate is  $29 F_o$  photons  $\text{cm}^{-2} \text{ s}^{-1}$ . These photons have a range of energies, but the vast majority of photons are around 20 eV. From this we can calculate a heating flux:  $20 \text{ eV} \times 29 n_o v_s \approx 2 \text{ erg cm}^{-2} \text{ s}^{-1}$ .

However, photons of energy 20 eV can only penetrate a column density of  $\sim 3 \times 10^{17} \text{ cm}^{-2}$ . This is similar to the derived column density of CO, so the total gas column density must be much larger. Hence, UV photons cannot penetrate and heat the full gas column.

#### X-ray heating

Both the forward and reverse shock, when traveling through tenuous gas, create a hot plasma that will slowly cool through X-rays. The average observed X-ray luminosity over the remnant is  $5.5 \times 10^{37} \text{ erg s}^{-1}$  (Hartmann et al., 1997). Dividing this by the size of the remnant ( $\sim 4'$  at 3.4 kpc), we find an X-ray heating flux of  $0.2 \text{ erg cm}^{-2} \text{ s}^{-1}$ . These photons have a typical energy of  $\sim 2 \text{ keV}$ , meaning they can heat a larger column density ( $\sim 3 \times 10^{19} \text{ cm}^{-2}$ ) than the UV photons.

#### Electron conduction

The hot shocked plasma could also heat the dense knot via heat conduction. The classical expression for heat conduction by electrons gives

$$Q = K(T) \frac{dT}{dr} \quad (3.1)$$

where  $K(T)$  is roughly constant and equal to  $\sim 6 \times 10^{-7} T^{5/2} \text{ erg s}^{-1} \text{ K}^{-7/2} \text{ cm}^{-1}$  (Tielens, 2005, p. 448–449). Note that this classical expression requires that the mean free path of the electrons is small compared with the length scale of the temperature gradient. For the parameters we adopt, this is indeed the case with a mean free path of  $\sim 10^{12}$  cm and a length scale of  $5 \times 10^{13}$  cm.

Setting the temperature gradient equal to  $T/\delta R$  with the temperature  $T=10^7$  K and the length scale  $\delta R$  given by the gas column density divided by the gas density,  $N/n = 5 \times 10^{13}$  cm, we find an energy flux of  $\sim 4 \times 10^4 \text{ erg cm}^{-2} \text{ s}^{-1}$ . This exceeds the UV and X-ray heating flux by several orders of magnitude, and is thus most likely the main heating mechanism.

Heat conduction is, however, extremely temperature sensitive. If the temperature of the hot plasma were decreased by an order of magnitude, to  $10^6$  K, the energy flux would be only  $\sim 10 \text{ erg cm}^{-2} \text{ s}^{-1}$ . This still surpasses the other heating mechanisms, but not by nearly as much.

The heat conduction energy into the knot will be balanced by mass evaporation from the surface of the knot. The mass-loss rate of the knot will be

$$\dot{M}_k = \frac{16\pi}{25} \frac{\mu}{k_B} K(T) T_h^{5/2} R_k \quad (3.2)$$

where  $\mu$  is the average mass of the gas (taken to be  $16 \text{ Da}^2$ , for an oxygen gas),  $T_h$  is the temperature of the hot electrons (here taken to be  $10^7$  K), and  $R_k$  the size of the knot. For our CO knot we find  $\dot{M}_k \sim 6 \times 10^{-5} M_\odot \text{ yr}^{-1}$ , corresponding to an evaporation time of  $\sim 2000$  years. The shock will take only  $\sim 50$  years to cross the knot, so the knot will not evaporate significantly during the shock interaction.

### 3.2.2 Future prospects

An important aspect of the CO gas in Cas A which is not constrained by our *Herschel* observations (beam  $\sim 50''$ ) is the knot size. In our analysis a knot size of  $0.5''$  was assumed, based on the  $<1''$  size limit from Rho et al. (2009), and similar constraints from optical observations. A larger knot size would significantly change the derived physical parameters of the gas. In order to constrain the knot size high angular resolution observations are required, and interferometry is the ideal method for reaching such resolution. As Cas A is in the Northern hemisphere it can not be observed with ALMA, so instead we will turn to the Plateau de Bure (PdBI) and Submillimeter Array (SMA) interferometers.

However, radio interferometers cannot probe the high-J CO transitions observed with *Herschel*, and following *Herschel's* end-of-life in April 2013 it will be difficult to observe the warm CO gas. On the other hand, the short CO cooling times suggests there should be a reservoir of cool CO gas, directly related to the

---

<sup>2</sup>Dalton or unified atomic mass unit, defined as one twelfth of the mass of a neutral carbon-12 atom.

observed warm gas. This cool gas can be observed with low-J CO transitions, and hence also with radio telescopes. As a first step towards this goal, with the intent of proving the existence of this cool gas reservoir, we obtained time at the IRAM 30m telescope to look for CO 2–1 at the same position as our *Herschel* observations. About half the allotted observing time has currently been completed, with no line detection so far.

Further continuation of the study of Cas A could involve the observation of multiple points within the remnant, at and around the reverse shock, to probe the gas parameters under various conditions. This would similarly be done with low-J CO transitions. Another possibility is to look for other molecules in Cas A, like SiO or SiS, which are predicted to be abundant in supernova ejecta. This will allow us to probe different gas properties, and to test the chemical model abundance predictions (e.g., Sarangi & Cherchneff, 2013). SiO, in particular, will provide a more direct link to the dust formation in the ejecta as it is a dust precursor.

An extension of the work on Cas A is to search for molecules in other supernova remnants. There are few remnants young and nearby enough to allow us to distinguish the ejecta from ISM material, but the famous SN 1987A is one of them. CO and SiO have already been discovered in its ejecta (Kamenetzky et al., 2013), so it is a prime candidate for the search for other molecules such as SiS or SO. Finding molecules in SN 1987A, and comparing their abundances, would provide a test of molecular model predictions.



# Bibliography

- Aitken, D. K., Smith, C. H., James, S. D., et al. 1988, MNRAS, 235, 19P
- Barlow, M. J., Krause, O., Swinyard, B. M., et al. 2010, A&A, 518, L138
- Beelen, A., Cox, P., Benford, D. J., et al. 2006, ApJ, 642, 694
- Bertoldi, F., Carilli, C. L., Cox, P., et al. 2003, A&A, 406, L55
- Borkowski, K. J. & Shull, J. M. 1990, ApJ, 348, 169
- Castro-Carrizo, A., Quintana-Lacaci, G., Bujarrabal, V., Neri, R., & Alcolea, J. 2007, A&A, 465, 457
- Cherchneff, I. & Dwek, E. 2009, ApJ, 703, 642
- Danziger, I. J., Fosbury, R. A. E., Alloin, D., et al. 1987, A&A, 177, L13
- de Jager, C. 1998, A&A Rev., 8, 145
- de Jager, C. & Nieuwenhuijzen, H. 1997, MNRAS, 290, L50
- Gall, C., Hjorth, J., & Andersen, A. C. 2011, A&A Rev., 19, 43
- Garcia-Segura, G., Langer, N., & Mac Low, M.-M. 1996, A&A, 316, 133
- Hartmann, D. H., Predehl, P., Greiner, J., et al. 1997, Nuclear Physics A, 621, 83
- Henize, K. G. 1976, ApJS, 30, 491
- Hutsemékers, D., Cox, N. L. J., & Vamvatira-Nakou, C. 2013, A&A, 552, L6
- Kamenetzky, J., McCray, R., Indebetouw, R., et al. 2013, ApJ, 773, L34
- Kotak, R., Meikle, P., Pozzo, M., et al. 2006, ApJ, 651, L117

- Kotak, R., Meikle, P., van Dyk, S. D., Höflich, P. A., & Mattila, S. 2005, *ApJ*, 628, L123
- Kotak, R., Meikle, W. P. S., Farrah, D., et al. 2009, *ApJ*, 704, 306
- Lagadec, E., Zijlstra, A. A., Oudmaijer, R. D., et al. 2011, *A&A*, 534, L10
- Le Bertre, T., Heydari-Malayeri, M., Epchtein, N., Gouiffes, C., & Perrier, C. 1989, *A&A*, 225, 417
- Lucy, L. B., Danziger, I. J., Gouiffes, C., & Bouchet, P. 1989, in *Lecture Notes in Physics*, Berlin Springer Verlag, Vol. 350, IAU Colloq. 120: Structure and Dynamics of the Interstellar Medium, ed. G. Tenorio-Tagle, M. Moles, & J. Melnick, 164
- Matsuura, M., Dwek, E., Meixner, M., et al. 2011, *Science*, 333, 1258
- Moseley, S. H., Dwek, E., Glaccum, W., Graham, J. R., & Loewenstein, R. F. 1989, *Nature*, 340, 697
- Oudmaijer, R. D., Davies, B., de Wit, W.-J., & Patel, M. 2009, in *Astronomical Society of the Pacific Conference Series*, Vol. 412, *The Biggest, Baddest, Coolest Stars*, ed. D. G. Luttermoser, B. J. Smith, & R. E. Stencel, 17
- Rho, J., Jarrett, T. H., Reach, W. T., Gomez, H., & Andersen, M. 2009, *ApJ*, 693, L39
- Rho, J., Kozasa, T., Reach, W. T., et al. 2008, *ApJ*, 673, 271
- Rho, J., Onaka, T., Cami, J., & Reach, W. T. 2012, *ApJ*, 747, L6
- Sarangi, A. & Cherchneff, I. 2013, *ArXiv e-prints*
- Sugerman, B. E. K., Ercolano, B., Barlow, M. J., et al. 2006, *Science*, 313, 196
- Szalai, T. & Vinkó, J. 2013, *A&A*, 549, A79
- Tielens, A. G. G. M. 2005, *The Physics and Chemistry of the Interstellar Medium*
- Todini, P. & Ferrara, A. 2001, *MNRAS*, 325, 726
- van der Tak, F. F. S., Black, J. H., Schöier, F. L., Jansen, D. J., & van Dishoeck, E. F. 2007, *A&A*, 468, 627
- Wallström, S. H. J., Biscaro, C., Salgado, F., et al. 2013, *A&A*, 558, L2
- Wilson, T. L. 2009, *Introduction to Millimeter/Sub-Millimeter Astronomy*. ArXiv e-print, to be published in the Saas Fee Winter School 2008.